Catalysis Today 148 (2009) 335–340

Contents lists available at ScienceDirect

Catalysis Today

journal homepage: www.elsevier.com/locate/cattod

Photocatalytic reduction of CO_2 with H_2O on Pt-loaded TiO_2 catalyst

Qin-Hui Zhang *, Wen-Dong Han, Yi-Juan Hong, Jian-Guo Yu *

State Key Lab of Chemical Engineering, College of Chemical Engineering, East China University of Science and Technology, Shanghai 200237, PR China

ARTICLE INFO

Article history:
Available online 18 August 2009

Keywords:
H_2O
CO_2 chemical reduction
Solar energy
TiO_2
Photocatalysis

ABSTRACT

A gas–solid heterogeneous system for solar–chemical energy conversion of CO_2-SCR (Selective Catalytic Reduction) with H_2O on different nanostructure photocatalysts and the photocatalysis pathway were discussed. Different crystal phases and sizes of low-dimensional nano-TiO_2 and Pt-metal supported photocatalysts are synthesized and characterized with X-ray diffraction, high-resolution transmission electron microscopy, photoluminescence, CO pulse chemisorptions, N_2 adsorption–desorption analysis at 77 K and X-ray fluorescence spectrometry. The catalytic activity was tested in a fixed-bed photocatalysis reactor and the CH_4 yield on the Pt/TiO_2 nanotube photocatalysts is more remarkable. It increased with the increase of the UV irradiation time and accumulated to about 4.8 $\mu mol\ h^{-1}\ g_{Ti}^{-1}$, enhanced as the increase of the reaction temperature and H_2O/CO_2 molar ratio as well.

1. Introduction

The conversion of CO_2 into useful substances is essential in developing alternative fuels and various raw materials for different chemical industries. It also aids in preventing the continuous rise in global temperature due to the green house effect of CO_2. However, CO_2 conversion always requires severe conditions of high pressure and/or high temperature since its stability and the activation of CO_2 to high-potential carbon compounds requires about 220–330 $kJ\ mol^{-1}$ energy thermodynamically [1], besides the contradiction that the supply of activation energy with fossil fuels inevitably produces CO_2 itself. In comparison, the solar reforming of CO_2 via photocatalytic reduction process is relatively more manageable and the specificity for the formation of CH_4, CO, CH_3OH, HCHO, HCOOH, etc., made it more attractive in fundamental research, which could also be one of the most desirable goals for storage of the solar energy if the UV band in the solar radiation is the only source used to power the reduction process.

Pioneering study on recycling CO_2 into useful products via semiconductors in aqueous suspension system was reviewed by Halmann [2], and recent research on the heterogeneous photocatalytic reduction of CO_2 with water vapour was summarized by Anpo et al. [3]. These summaries provided fundamental information essential to photoreduction of CO_2 through catalytic process. TiO_2, with the low band-gap values of about 3.0 and 3.2 eV for rutile and anatase phase respectively, could fulfil the thermodynamic requirements of most photocatalytic reactions investigated and it is reasonably cheap, photo-stable and non-toxic, making it a perfect candidate for photocatalytic process. Many noble metals or transition metals impregnated TiO_2, including Pt and Cu, could prevent the recombination of the photo-generated electron–hole pairs so as to enhance the photocatalytic activity of TiO_2, and the loading content of metals is also important since high content metal will induce faster electron–hole recombination and deactivate the photocatalyst soon [4–7]. It will also influence the selectivity of CH_4 or CH_3OH formation, Tseng and Wu found that Cu could improve the CH_3OH yield and the isolated Cu^{1+} was regarded as the primary active site [7], while, Slamet et al. thought that Cu^{2+} supported on TiO_2 have more significant contribution to improve the CO_2 photocatalytic reduction activity [8]. Although some investigators noted that Pt dispersed on TiO_2 could improve the photocatalytic activity of TiO_2 [4,9], the systematic research about the effect of Pt-metal supported on TiO_2 to produce CH_4 via the photocatalytic reduction of CO_2 with gaseous H_2O is still requisite.

Thus in this paper, a series of Pt-loaded nano-TiO_2 (nanoparticle and nanotube) photocatalysts were synthesized via high temperature hydrothermal and incipient wet impregnation method. The catalysts were characterized by X-ray diffraction (XRD), high-resolution transmission electron microscopy (HRTEM), photoluminescence, CO pulse chemisorptions, N_2 adsorption–desorption analysis and X-ray fluorescence spectrometry (XRF). The catalytic activity was tested via the reduction of CO_2 with gaseous water in a fixed-bed photocatalysis reactor and the photocatalysis pathway was further discussed.

* Corresponding author. Tel.: +86 21 64252171; fax: +86 21 64252826.
E-mail addresses: qhzhang@ecust.edu.cn (Q.-H. Zhang), jgyu@ecust.edu.cn (J.-G. Yu).

0920-5861/$ – see front matter © 2009 Elsevier B.V. All rights reserved.
doi:10.1016/j.cattod.2009.07.081

2. Experimental

2.1. Catalyst preparation

All chemicals used in this work were AR reagents, except where otherwise indicated. TiO_2 (P25, a highly dispersed titanium oxide from Degussa) was entitled TO-NP in the experiment. Low-dimensional TiO_2 nanotube (TO-NT) was produced via high temperature hydrothermal methods. TO-NP (5 g) and an aqueous solution of NaOH (10 mol l^{-1}, 500 ml) were mixed for 0.5 h in an ultrasonic bath, then transferred into a Teflon-lined stainless steel autoclave, sealed, and maintained at 448 K for 48 h; after the reaction was completed, the resulted white precipitate was separated by filtration and washed with 0.1 mol l^{-1} HCl solution and deionised water until the conductance of the supernatant lucid solution reached the same level with the deionised water (the pH value now was about 7.0), followed by ultrasonic assisted dispersion in anhydrous ethanol for 0.5 h and dried at 333 K for 8 h. Pt/TO-NP and Pt/TO-NT catalysts were prepared by incipient wet impregnation method with an aqueous solution of $H_2PtCl_6{\cdot}6H_2O$. An appropriate amount of $H_2PtCl_6{\cdot}6H_2O$ solution based on Pt content in the sample (0.05, 0.1 and 0.2 wt.%) was mixed with TO-NP in distilled flask. The resulting slurry was stirred in the rotary dryer at 333 K for 2 h and maintained at 363 K for 30 min to evaporate the water completely. The solid residue is further dried at 383 K for 12 h and calcined in air at 773 K for 2 h. Before the catalyst activity test, it was reduced in 30 ml/min 5% H_2/N_2 flow at 723 K for 3 h. The preparation of 0.1 wt.% Pt/TO-NT catalyst was prepared with the similar procedure.

2.2. Catalyst characterization

The crystal phase of the support and final catalyst were analysed by Rigaku D/max 2550 X-ray diffractometer using Cu Kα radiation (λ = 1.54056 Å) with the scan range of 2θ = 10–80°and operating at 40 kV, 100 mA. The weight content of Pt loaded in the catalyst was measured by Shimadzu XRF-1800 with a Ru Kα conducted at 40 kV, 95 mA, and the element content was calculated by fundamental parameter (FP) method [10]. The pore structure of the catalysts were characterized by N_2 adsorption at 77 K using an adsorption apparatus (Micromeritics, ASAP 2010 V5.02), the surface area of the samples was determined from the Brunauer–Emmett–Teller (BET) equation and pore volume, from the total amount of nitrogen adsorbed at relative pressures of ca. 0.96. The microstructure and morphology of the samples were analyzed using a JEOL JEM-2100F TEM (200 kV) after the samples were dispersed by ultrasonic in anhydrous ethanol for 10 min and then placed onto the Cu grid for observations. The photoluminescence spectra of the catalysts were measured using a Fluorescence Spectrophotofluorometer (VARIAN Cary Eclipse) to investigate the sensitivity of the photocatalysts to the excitation signal at room temperature. The Pt-metal dispersion of the catalyst was determined by CO Pulse Chemisorptions Analysis (Micromeritics, AutoChem II 2920) and calculated according to Eq. (1) [11], assuming that the CO molecules adsorbed on the Pt-metal surface were in agreement with top site adsorption configuration, so that the amount of surface Pt sites were equal to the number of adsorbed CO on Pt atoms.

$$D = 100 \times \frac{\mathrm{GMWcalc}(\mathrm{Vs} \times \mathrm{SFcalc})}{(\mathrm{SW} \times 22,414)} = \frac{0.87\mathrm{Vs}}{\mathrm{SW}} \quad (1)$$

D: percent metal dispersion;
GMWcalc: gram molecular weight of metal (g mol^{-1});
Pt: 195.09 g mol^{-1};
Vs: volume sorption (ml, STP);
SFcalc: calculate stoichiometry factor, SFcalc = 1;
SW: sample weight (g).

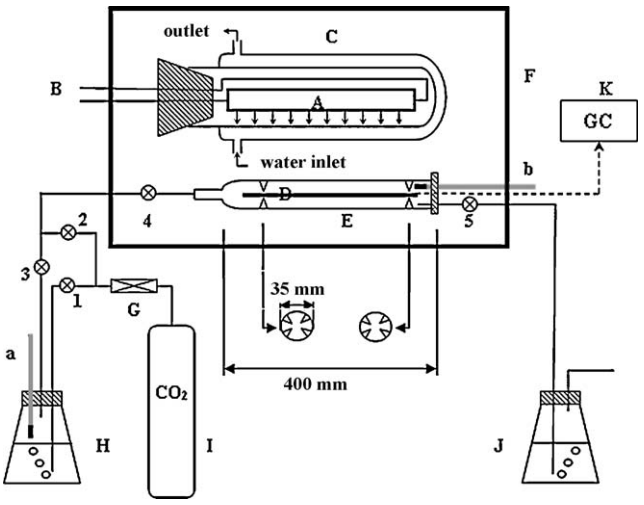

Fig. 1. The set-up of the fixed-bed photocatalysis reactor A – UV/visible light; B – electrical wire; C – U-type terrarium; D – quartz glass plate; E – quartz glass reactor; F – insulation chest; G – gas flowmeter; H – conical flask for deionised water; I – CO_2 gas; J – absorption flask; K – gas chromatography; 1–5 – Valve; a, b – thermometer.

2.3. Catalyst test

A fixed-bed photocatalytic reactor was designed as shown in Fig. 1 of the experimental set-up. The main part of the experimental rig is a cylindrical quartz glass tube reactor. A flat quartz glass plate was integrated in the tube to hold the catalysts. The reactor has the size of 400 mm (length) × 35 mm (outside diameter) and the net volume of 265 ml. UV light system includes a 300 W high-pressure Hg lamp (wavelength 365 nm) and a U-type quartz terrarium. The cooling water flows through the interlayer of the terrarium to remove the heat resulting from the long UV irradiation time. The photocatalytic reduction of CO_2 with gaseous H_2O was carried out with catalysts (50 mg) on the flat quartz plate in the reactor. Before the UV irradiation, CO_2 (99.5% purity) was first flowed through the reactor to ensure the air was eliminated; secondly, switch the valves to make CO_2 flowed through deionised water in conical flask at first, and then flow into the reactor. The amount of H_2O vapour in the feed stream (H_2O/CO_2 molar ratio) was regulated by the temperature of the water in the conical flask. Third, turn off the valves to make the whole system tightly sealed and turn on the UV light lamp to start the photoreaction process. Analysis of the feed stream and the product mixtures was performed with an Agilent 6890 N gas chromatograph with HP-PLOT Q column (30 m × 0.535 mm × 40 μm) and flame ionisation detectors.

3. Results and discussion

3.1. Morphological structure and texture of the catalysts

The weight content of Pt in TiO_2 nanoparticle (TO-NP) and TiO_2 nanotube (TO-NT) catalysts were 0.12 and 0.15%, respectively, calculated from the XRF measurement, which had little differences with the initially designed Pt-metal loading content of 0.1%. Therefore, the catalysts were entitled 0.12Pt/TO-NP and 0.15Pt/TO-NT accordingly.

Fig. 2 shows the XRD spectra of the samples. For the TO-NP sample, the peaks at 2θ = 25.2°, 37.9°, 48.3°, 53.9°, 55.0°, 62.7°, 68.9°, 70.1° and 75.5° were identified as anatase phase of TiO_2, and the other diffraction peaks at 2θ = 27.5°, 36.1°, 41.3° and 48.1° represented rutile phase of TiO_2 structure. The content of antatase

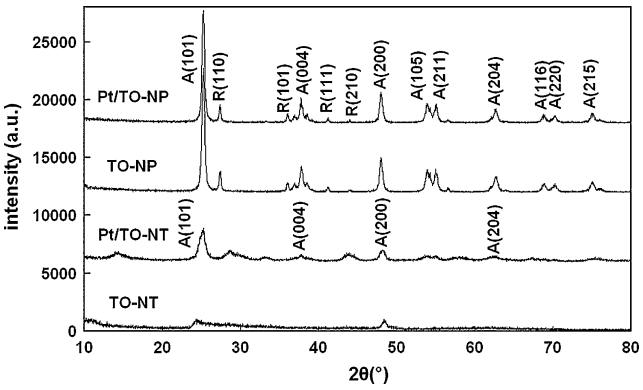

Fig. 2. XRD patterns of TiO_2 nanotube (TO-NT), 0.15Pt/TO-NT, TiO_2 nanoparticle (TO-NP), and 0.12Pt/TO-NP samples.

phase was analyzed via the usually accepted quantitative method [12] as Eq. (2) with the relative peak intensity of the anatase (1 0 1) crystal face (d = 3.520 Å) and the rutile (1 1 0) crystal face (d = 3.247 Å), in which, F_R was the mass fraction of rutile phase of titania, I_A and I_R, the integrated intensities of the anatase (1 0 1) and rutile (1 1 0) crystal face of titania, respectively. According to this equation, the mass fraction of anatase phase in the TO-NP sample was calculated to be 85.32%.

$$F_R = \frac{1}{1 + 1.26(I_R/I_A)} \quad (2)$$

The relatively broad Bragg peaks of TO-NT could not be assigned to the anatase, rutile or any known phase of TiO_2 in JCPDS card. In many related reports to analyze the structure of the low dimension nanostructures, similar phenomena were discovered and described as $H_2Ti_3O_7{\cdot}xH_2O$ [13–15], $Na_xH_{2-x}Ti_3O_7$ [16], $H_2Ti_4O_9{\cdot}H_2O$ [17], and $H_2Ti_2O_4(OH)_2$ [18], yet, it was preferred to be indexed as $H_2Ti_3O_7$ according to current structure investigations since we carefully compared the synthesis process with those in the related literature, and confirmed the point of view of Sun and Li [16] and Kasuga et al. [19,20] that the washing and dispersing process was key to obtain the TiO_2 tubular structure. In such earlier reports on one-dimensional titania nanotubes, the washing process merely with water would result mainly vesicles, shrinking under irradiation with an electron beam and finally changing to aggregate-like depositions. In this case, anhydrous ethanol was used to disperse the white precipitate after washing with HCl solution and deionised water, and typical HRTEM image was shown in Fig. 3. Samples dispersed in ethanol yielded mainly monodispersed nanotubes with Ø20 nm (out diameter) × 300 nm (length) × 5 nm (thickness), implying that ethanol was a good dispersant and aided the formation of low-dimensional TiO_2 nanotube. Additionally, the use of ethanol enabled the formation of aggregation-free TiO_2 nanotubes with quite uniform geometry, evidenced by the pore size distribution obtained from the Barrett–Joyner–Halenda (BJH) deposition curve (inset of Fig. 4c), indicating that the ethanol washed and dispersed nanotubes maintained a pore size distribution centred around 18 nm, with no other peaks in the range from 1 to 100 nm. The pore size distribution, unlike the HRTEM observations, was obtained statistically, thus the appearance of the single broad peak was attributed to capillary condensation in the slit-shaped mesopores with parallel walls and implied the separation of most nanotubes from one another although some of the nanostructures looked thicker than others.

For both the Pt-metal loading catalysts, the Pt-metal diffraction signals were not found since their ultra fine dispersion on TiO_2 particles as very small particles as shown in the HRTEM images of Fig. 3 and the very low Pt-metal content calculated from XRF result. The TO-NP oxide and 0.12Pt/TO-NP catalyst had the similar XRD patterns, while the diffraction pattern of 0.15Pt/TO-NT sample could be readily indexed to anatase TiO_2, indicating that the crystal phase transformed to anatase phase after calcination treatment in Pt-metal impregnation process.

The HRTEM images of 0.12Pt/TO-NP and 0.15Pt/TO-NT catalysts were shown in Fig. 3. Small particles that were homogeneous in size (average 20–50 nm) and shape could be observed from Fig. 3a and the small dark spots on the TiO_2 nanoparticles presented the Pt-metal particles with the size of 1–2 nm distributed on the TiO_2 particles. Fig. 3b shows the TiO_2 nanotube with Ø20 nm (out diameter) × 300 nm (length) × 5 nm (thickness) prepared via soft-chemistry hydrothermal method and most Pt-metal particles loaded in the inner part of the nanotubes which was still stable at 723 K. The research on the effect of Pt-metal loaded in the inner or outer part of the nanotubes was still in process.

Fig. 4 shows the N_2 adsorption–desorption isotherms and insets of pore size distribution curves of the samples. The specific surface area of 0.12Pt/TO-NP was 48.56 $m^2\ g^{-1}$, which decreased compared to the starting material TO-NP (S_{BET} = 101.34 $m^2\ g^{-1}$) after the Pt-metal impregnation process. Pore size distribution analysis via the density functional theory (DFT) method, applicable for a complete range of pore size, was inserted in Fig. 4. TO-NP and 0.12Pt/TO-NP afforded a similar mesoporous size distribution with the peak pore size (D_p) centred around 38 nm. TO-NT sample had a large specific surface area (252.86 $m^2\ g^{-1}$), and the adsorption–desorption isotherm (Fig. 4c) contained an obvious H2-type hysteresis loop with a highly delayed desorption branch resulted from the hollow structure of the nanotube also indicated in the HRTEM images of Fig. 3. The loading of Pt-metal also decreased the special surface area of nanotube to 92.26 $m^2\ g^{-1}$. The D_p of TO-NT was around 18 nm, and after the Pt-metal impregnation process the D_p increased to about 30 nm resulted from recrystallization of TiO_2 to anatase phase.

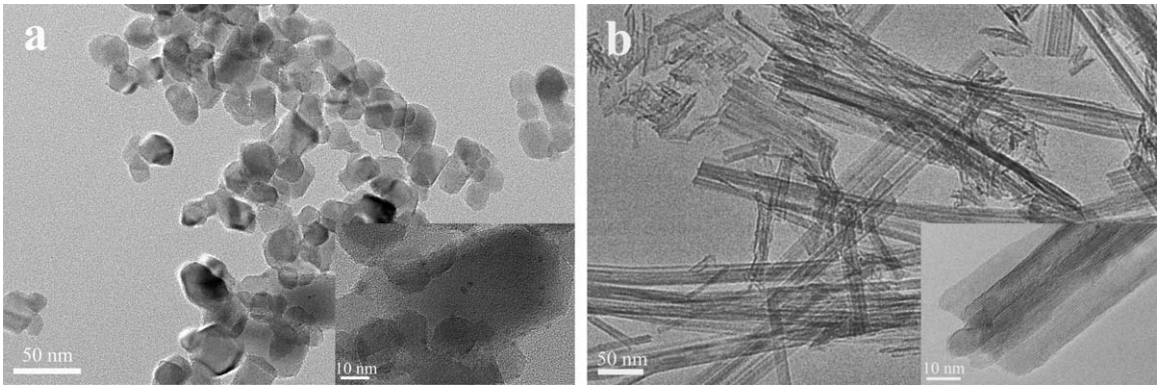

Fig. 3. HRTEM images of 0.12Pt/TO-NP (a) and 0.15Pt/TO-NT (b) catalysts.

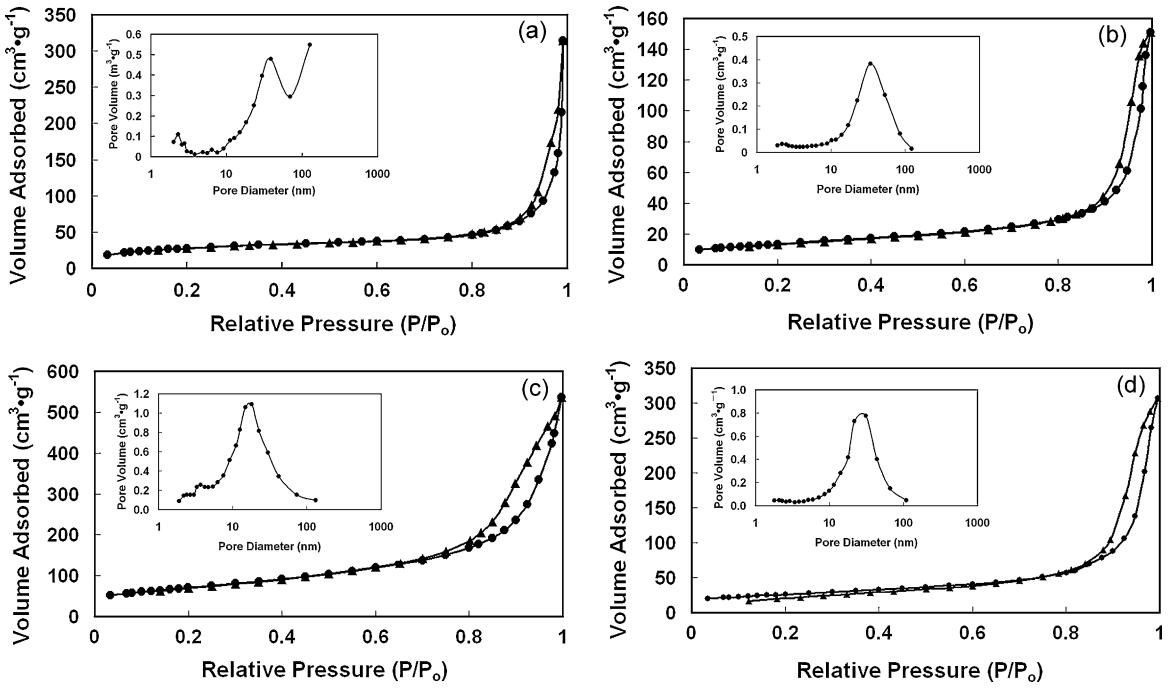

Fig. 4. N_2 adsorption–desorption and pore size distribution curves (insert) of: (a) TiO_2 nanoparticle (TO-NP), (b) 0.12Pt/TO-NP, (c) TiO_2 nanotube (TO-NT), and (d) 0.15Pt/TO-NT samples.

Table 1
Physicochemical properties of the support and photocatalyst reduced at 723 K.

Sample	Pt-load (wt.%)[a]	BET surface (m^2/g)	Pt disp. (%)[b]	Pt size (nm)[c]	Pt size (nm)[d]	TiO_2 size (nm)[d]
TO-NP	/	101.34	/	/	/	20–50
TO-NT	/	252.86	/	/	/	Ø20 (out diameter) × 300 (length) × 5 (thickness)
Pt/TO-NP	0.12	48.56	88.59	1.3	1–2	20–50
Pt/TO-NT	0.15	92.26	92.15	1.2	1–2	Ø20 (out diameter) × 300 (length) × 5 (thickness)

[a] Measured from X-ray fluorescence analysis.
[b] Dispersion of Pt-metal obtained from CO pulse chemisorption.
[c] Particle size of Pt-metal calculated with the empirical formula of $d = 1/\text{dispersion}$.
[d] Particle size of the oxide measured by HRTEM.

The physicochemical properties of the catalysts were summarized in Table 1. It should be realized that the particle sizes of Pt-metal estimated from the Pt-dispersion data of the reduced Pt/TO-NP and Pt/TO-NT catalysts were comparable to the HRTEM images.

The samples were demonstrated to be photoactive as evidenced by the photoluminescence spectra (Fig. 5). Emissions around 510–530 nm were observed for the catalysts at room temperature with excitation at 260 nm. This behavior was noteworthy because the observed photoluminescence spectra were attributed to the radiative decay process from the charge transfer excited state formed in the excitation process to the ground state of the photocatalyst [21], and the photoluminescence intensity was in the order of TO-NT < TO-NP < 0.12Pt/TO-NP < 0.15Pt/TO-NT. The photoluminescence intensity of Pt-loaded TiO_2 catalysts was stronger than that of the TiO_2 oxides without Pt-metal, indicating that the loading of Pt-metal could transmit the excited electrons and delay the recombination of the excited electron-hole pairs to improve UV light utilization efficiency, and the intensity could increase with the Pt-metal content loaded in the TiO_2 oxides.

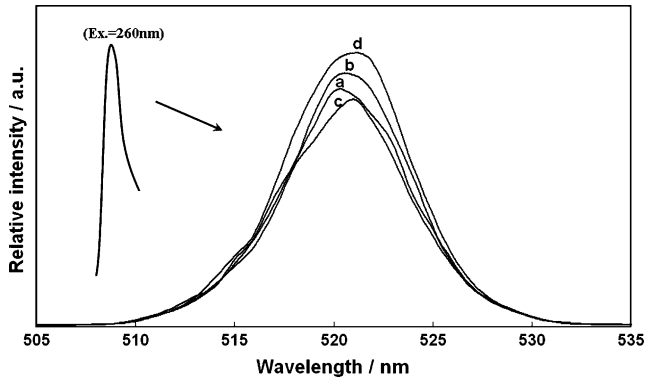

Fig. 5. Photoluminescence spectrum of (a) TiO_2 nanoparticle (TO-NP), (b) 0.12Pt/TO-NP, (c) TiO_2 nanotube (TO-NT) and (d) 0.15Pt/TO-NT, excitation at 260 nm.

3.2. Photocatalytic activity

There was no product detected under dark conditions or with UV irradiation without the photocatalyst when the other reaction conditions remained the same, indicating that the presence of both photocatalyst and UV irradiation were necessary for the process of photocatalytic reduction of CO_2 with gaseous H_2O.

TiO_2 nanoparticle oxides (TO-NP) had no activity in photocatalytic reduction of CO_2 with gaseous H_2O as the reactor maintained at 323 K. However, Pt/TO-NP with different Pt-metal content could photocatalyse the reduction of CO_2 with H_2O vapour well. Fig. 6 shows that CH_4 yield in photocatalytic reduction of CO_2

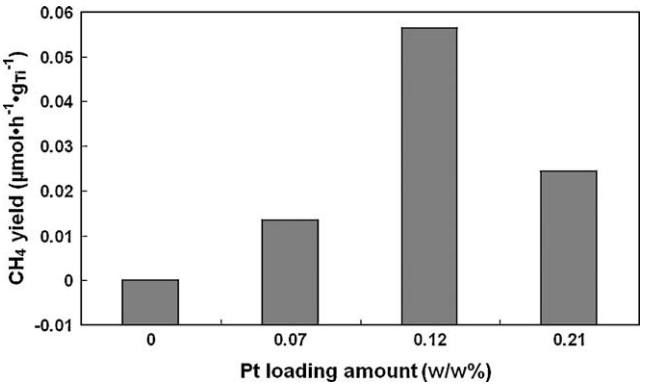

Fig. 6. Effect of Pt-metal content in Pt/TO-NP catalysts on CH_4 yield for photocatalytic reduction of CO_2 after 7 h UV irradiation at 323 K, H_2O/CO_2 = 0.02.

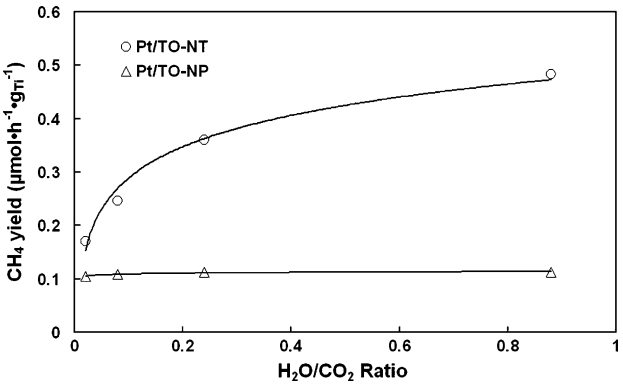

Fig. 9. Effect of H_2O/CO_2 molar ratio on CH_4 yield of 0.12Pt/TO-NP and 0.15Pt/TO-NT photocatalysts at 328 K with UV irradiation time = 17 h.

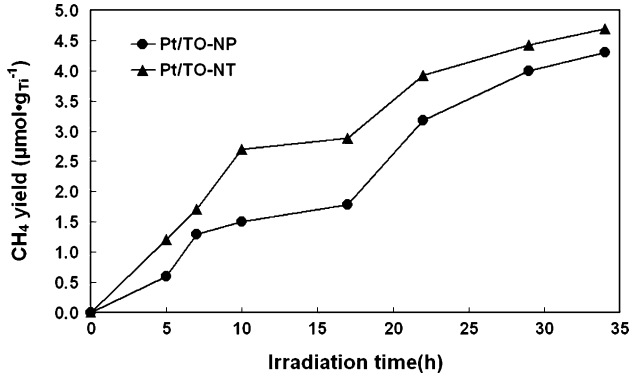

Fig. 7. Effect of UV irradiation time on CH_4 yield of 0.12Pt/TO-NP and 0.15Pt/TO-NT photocatalyst at 328 K, H_2O/CO_2 = 0.02.

with various amount of loaded Pt-metal on TiO_2 nanoparticles and 0.12Pt/TO-NP catalyst exhibited the highest activity on CH_4 yield with 0.0565 μmol h^{-1} $g_{Ti}{}^{-1}$ at the condition of H_2O/CO_2 = 0.02 (molar ratio) after 7 h UV irradiation.

The effect of UV irradiation time on the CH_4 yield over a wide period of 5–34 h was further investigated at 328 K and H_2O/CO_2 = 0.02 as shown in Fig. 7. The CH_4 yield on both photocatalysts increased with the increase of the UV irradiation time, and accumulated to about 4.8 and 3.9 μmol h^{-1} $g_{Ti}{}^{-1}$ for 0.15Pt/TO-NT 0.12 and Pt/TO-NP, respectively.

The catalysis activity of 0.12Pt/TO-NP and 0.15Pt/TO-NT was compared at the same reaction conditions of UV irradiation time = 17 h, H_2O/CO_2 = 0.02 (molar ratio), and reaction temperature at 323, 333, 343 K as shown in Fig. 8. It was obvious that the 0.15Pt/TO-NT had higher CH_4 yield than the 0.12Pt/TO-NT catalysts, and the CH_4 yield on both catalysts was enhanced as the increase of the reaction temperature. The increase of temperature was advantageous to the desorption process of products formed and enhance the chance of effective collisions [22] between the charge transfer excited state $[Ti^{3+}–O^-]^*$ species and the reactant molecules.

Fig. 9 shows the relationship between the CH_4 yield and the molar ratio of H_2O/CO_2 in the initial feed stream. The CH_4 yield on 0.15Pt/TO-NT increased with the relative large concentration of H_2O molecules surrounding the TiO_2 nanotube and high concentration of surface OH group as evidenced by Ikeue et al. [21] too. However, the different H_2O/CO_2 molar ratio had little effect on CH_4 yield of 0.12Pt/TO-NP photocatalyst.

3.3. Photocatalysis pathway

The pathway for photocatalytic reduction of CO_2 with gaseous H_2O to produce CH_4 on Pt/TiO_2 catalyst was proposed. As irradiated by UV light of suitable wavelength with sufficient photonic energy ($h\nu$), photo-generated electron–hole pairs and the charge transfer excited state $[Ti^{3+}–O^-]^*$ species were created [23], part of the excited electrons and holes recombined together and radiated out heat or light (as shown in Fig. 5) during the process, while other part that had not recombined would react with the adsorbed reactants on TiO_2 surface. Since Pt-metal had higher work function (Φ_m) than TiO_2 (Φ_s), some electrons transmitted via the Pt-metal and avoided the recombination with holes effectively to extend the life-span of the electron–hole pairs as shown in Fig. 10.

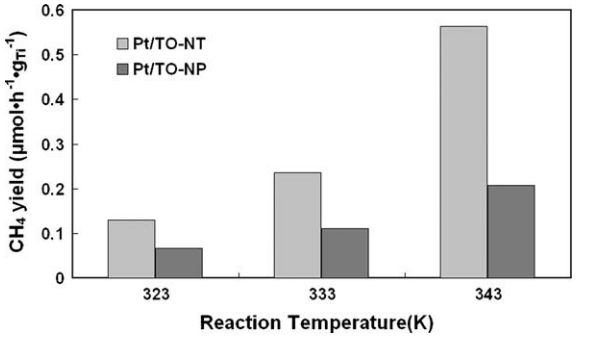

Fig. 8. CH_4 yield in the photocatalytic reduction of CO_2 on 0.12Pt/TO-NP and 0.15Pt/TO-NT photocatalyst at different reaction temperatures with UV irradiation time = 17 h and H_2O/CO_2 = 0.02 (molar ratio).

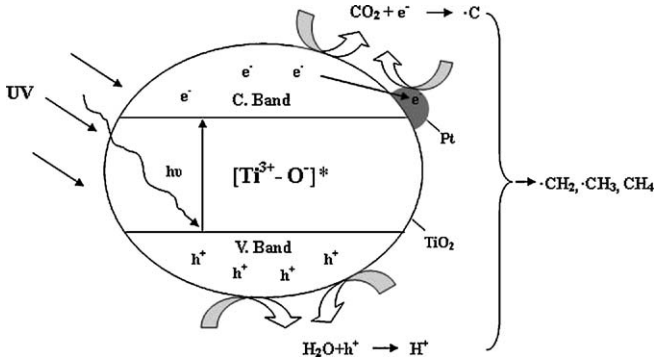

Fig. 10. Schematic of UV photo-excitation process on Pt/TiO_2 catalyst.

The excited holes reacted with adsorbed water vapour on the catalyst surface to produce hydroxyl radicals ($^{\bullet}OH$) and hydrogen ions (H^+), and further oxidized by $^{\bullet}OH$ radicals to produce O_2 and H^+ [24]; meanwhile, the charge transfer excited state $[Ti^{3+}–O^-]^*$ species reacted with adsorbed CO_2 to produce CO and O_2, and further reacted with CO to produce carbon radicals ($^{\bullet}C$) [23]. The carbon radicals then reacted with H^+ and e^- on the catalyst surface to produce intermediate $^{\bullet}CH_2$, $^{\bullet}CH_3$, and finally CH_4. The possible process would have undergone the following pathway:

$$[Ti^{4+}–O^{2-}] + h\nu \rightarrow h^+ + e^- + [Ti^{3+}–O^-]* \quad (3)$$

$$H_2O + h^+ \rightarrow {}^{\bullet}OH + H^+ \text{and} {}^{\bullet}OH + H_2O + 3h^+ \rightarrow O_2 + 3H^+ \quad (4)$$

$$CO_2 + [Ti^{3+}–O^-]* \rightarrow CO + 1/2O_2 \text{and} CO + [Ti^{3+}–O^-]* \rightarrow {}^{\bullet}C + 1/2O_2 \quad (5)$$

$$^{\bullet}C + H^+ + e^- \rightarrow {}^{\bullet}CH_2 \rightarrow {}^{\bullet}CH_3 \rightarrow CH_4 \quad (6)$$

4. Conclusions

A gas–solid heterogeneous reaction for solar–chemical energy conversion of CO_2-SCR with H_2O vapour on various nanostructure photocatalysts had been performed and CO_2 could be transformed into CH_4 as in contact with water vapour on Pt/TiO_2 catalysts under the UV irradiation at mild conditions of low pressure and temperature. The appropriate Pt-metal content could obviously improve the photocatalytic activity and Pt/TiO_2 nanotube was more active than Pt/TiO_2 nanoparticle catalyst. Although the CH_4 yield was not high enough to use as fuels currently, the Pt/TiO_2 catalyst was found to be feasible and attractive for use in further investigation of CO_2 photoreduction for CO_2 environment management.

Acknowledgements

The research received financial support by NSFC (20706014 & 20576031), STCSM (0852nm02100) and Key Project of Chinese Ministry of Education (108144).

References

[1] Y. Kohno, H. Hayashi, S. Takenaka, et al. J. Photochem. Photobiol. A: Chem. 126 (1999) 117.
[2] M. Halmann, Chemical Fixation of Carbon Dioxide: Methods for Recycling CO_2 into Useful Products, CRC Press, 1993,. p. 172.
[3] M. Anpo, H. Yamashita, in: M. Schiavello (Ed.), Heterogeneous Photocatalysis, vol. 3, Wiley, Chichester, New York, 1997, p. 133.
[4] O. Ishitani, C. Inoue, Y. Suzuki, T. Ibusuki, J. Photochem. Photobiol. A: Chem. 72 (1993) 269.
[5] L. Murruni, G. Leyva, M.I. Litter, Catal. Today 129 (2007) 127.
[6] N. Sasirekha, S.J.S. Basha, K. Shanthi, Appl. Catal. B: Environ. 62 (2006) 169.
[7] I.-H. Tseng, J.C.-S. Wu, Catal. Today 97 (2004) 113.
[8] H.W. Slamet, E. Nasution, S. Purnama, J. Kosela, Gunlazuardi, Catal. Commun. 6 (2005) 313.
[9] S.H. Chien, M.C. Kuo, C.H. Lu, K.N. Lu, Catal. Today 97 (2004) 121.
[10] E. Margui, I. Queralt, M. Hidalgo, Trends Anal. Chem. 28 (2009) 362.
[11] V. Perrichon, L. Retailleau, P. Bazin, M. Daturi, J.C. Lavallery, Appl. Catal. A: Gen. 260 (2004) 1.
[12] R.A. Spurr, H. Myers, Anal. Chem. 29 (1957) 760.
[13] G.H. Du, Q. Chen, R.C. Che, Z.Y. Yuan, L.M. Peng, Appl. Phys. Lett. 79 (2001) 3702.
[14] Q. Chen, W.Z. Zhou, G.H. Du, L.M. Peng, Adv. Mater. 14 (2002) 1208.
[15] Y. Suzuki, S. Yoshikawa, J. Mater. Res. 19 (2004) 982.
[16] X.M. Sun, Y.D. Li, Chem. Eur. J. 9 (2003) 2229.
[17] A. Nakahira, W. Kato, M. Tamai, et al. J. Mater. Sci. 39 (2004) 4239.
[18] M. Zhang, X.D. Wang, J.J. Zhang, J. Mol. Catal. A: Chem. 217 (2004) 203.
[19] T. Kasuga, M. Hiramatsu, A. Hoson, et al. Langmuir 14 (1998) 3160.
[20] T. Kasuga, M. Hiramatsu, A. Hoson, et al. Adv. Mater. 11 (1999) 1307.
[21] K. Ikeue, S. Nozaki, M. Ogawa, M. Anpo, Catal. Today 74 (2002) 241.
[22] S.S. Tan, L. Zou, E. Hu, Catal. Today 131 (2008) 125.
[23] H. Yamashita, H. Nishiguchi, N. Kamada, M. Anpo, Res. Chem. Intermed. 20 (1994) 815.
[24] S.S. Tan, L. Zou, E. Hu, Catal. Today 115 (2006) 269.